IEEE Photonics Journal
An IEEE Photonics Society Publication

Think Outside the Fiber: Imaging Amplifier for Space-Multiplexed Optical Transmission

Volume 4, Number 5, October 2012

Ibrahim Ozdur
Hong Shu
Michael Bass
Guifang Li

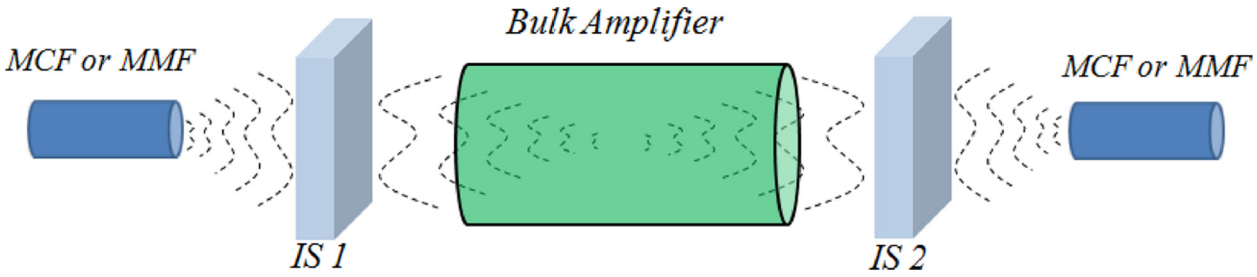

DOI: 10.1109/JPHOT.2012.2208184
1943-0655/$31.00 ©2012 IEEE

Think Outside the Fiber: Imaging Amplifier for Space-Multiplexed Optical Transmission

Ibrahim Ozdur,[1,2] Hong Shu,[1] Michael Bass,[1] and Guifang Li[1]

[1]CREOL: The College of Optics and Photonics, University of Central Florida, Orlando, FL 32816 USA
[2]Applied Communication Sciences, Red Bank, NJ 07701 USA

DOI: 10.1109/JPHOT.2012.2208184
1943-0655/$31.00 ©2012 IEEE

Manuscript received June 8, 2012; revised July 2, 2012; accepted July 3, 2012. Date of publication July 11, 2012; date of current version July 27, 2012. Corresponding authors: G. Li and I. Ozdur (e-mail: li@creol.ucf.edu; iozdur@appcomsci.com).

Abstract: This paper proposes a simple and practical method to amplify signals for space-multiplexed optical transmission. In this amplification technique, the output facet of the multicore or multimode fiber is mapped back to the same type of fiber after passing through an imaging and bulk amplifying region. Simulations are carried out for a seven-core multicore fiber with the signal lasers amplified by a bulk erbium–ytterbium-doped phosphate glass amplifier. Amplifier gain of ~20 dB is achieved at an input power of 6 mW for each individual core with an optical power conversion efficiency of 32.5%. The proposed amplifier technique does not have a core or mode count limit for multicore and multimode fibers.

Index Terms: Optical amplifiers, spatial division multiplexing, multicore fibers (MCFs).

1. Introduction

Fueled by emerging bandwidth-hungry applications and increases in computer processing power, Internet traffic has sustained exponential growth in recent years. Different multiplexing techniques, such as time-, wavelength-, and polarization-division multiplexing, have been investigated in detail, both theoretically and experimentally [1]–[5]. Another brute-force technique for a higher link capacity is to increase the fiber count in a fiber cable. However, size limitations and duct congestion problems limit the fiber count. In order to overcome the bandwidth problem, space-multiplexed optical transmission using multicore fibers (MCFs) [6], [7] and few-mode fibers (FMFs) [8] has been suggested. An FMF is a single-core large-area fiber that allows many spatial modes to travel inside, and an MCF is a fiber that has several cores. Recently, MCFs have attracted extensive interest due to their potential to multiply the capacity of a fiber, and promising results are obtained by different groups [9], [10]. However, space-multiplexed optical transmission remains limited to several tens of kilometers due to the lack of a practical amplification technique.

It is obvious that commercial erbium-doped fiber amplifiers (EDFAs) cannot be used *for* space-multiplexed transmission. The basic reason is that commercial EDFAs are based on single-mode fibers, which have only one degree of freedom (spatial mode), whereas multimode fibers (MMFs) or MCFs have many degrees of freedom. A straightforward way to provide signal amplification for an MCF is to separate the cores and then amplify each core individually using a dedicated single-mode EDFA. This straightforward method increases the degrees of freedom but also increases the number of required components by a factor equal to the number of cores (N), which means N pump sources, N wavelength-division multiplexing (WDM), N erbium-doped fiber (EDF), and N times the electronics.

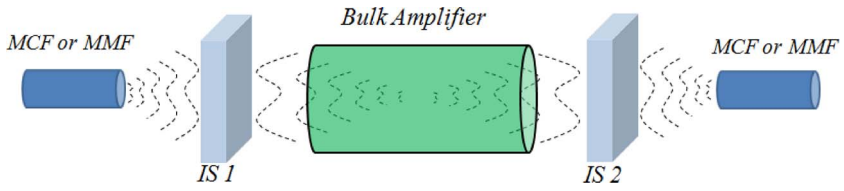

Fig. 1. General schematic of the imaging amplifier. (*MCF* and *MMF* are the multicore and multimode fibers; *IS* is the imaging system.)

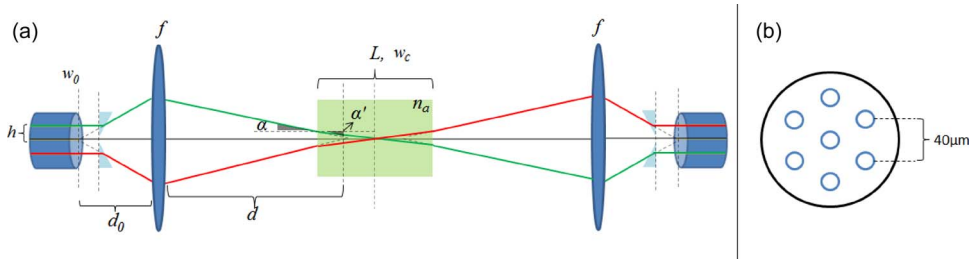

Fig. 2. (a) Detailed optical system setup used in the simulation. (b) Facet of the MCF.

In this paper, we propose a new amplification technique, which we call imaging amplification, for multicore and multimode fibers. In this technique involving both imaging and amplification, the facet of the input multicore or multimode fiber is imaged to the facet of the output fiber of the same type after passing through an amplifying region. It exploits the parallelism in bulk optics to provide the additional degrees of freedom necessary for the amplification of multicore and multimode fibers. The method is simulated for a seven-core fiber by using an erbium–ytterbium-doped phosphate glass. The simulation resulted in a ∼20-dB gain of the individual cores.

2. Proposed Imaging Amplifier

A general schematic of the imaging amplifier can be found in Fig. 1.

As shown in Fig. 1, the signal from the output facet of the multicore or multimode fiber is imaged to another same type of fiber after passing through a bulk amplifier. Imaging systems (*IS 1* and *IS 2*) are necessary to focus/collimate the beam at the center of the bulk amplifier and then coupling back to the output fiber. The imaging system designs for MMFs are relatively straightforward and can be made by using single-lens pairs. Whereas, the imaging system for the MCFs requires more complex designs and optimization in order to achieve low pump power. For example, a simple and well-known method to image the output facet of an MCF onto another one is the 4-f optical system; however, this system requires very high pump power to obtain ∼20-dB gain and, hence, is not preferred.

Fig. 2(a) shows the optical system in detail that is used in the simulations. A vertically positioned three-core fiber is shown as a visual aid. The core pitch (h) is assumed to be 40 μm, and the beam waist at the output of the fiber is 5 μm. The beams coming from the MCF are tilted by using a wedge prism with index of refraction of 1.5 and angle $\sim 20.4^\circ$ and then sent to a single lens with focal length $(f) = 5$ mm. The distance between the MCF and the lens (d_o) is ∼5.35 mm. After the lens, the beams are directed to a focusing point (d) of ∼74 mm with an angle (α) of $\sim 0.82^\circ$. The refractive index (n_a) and the length (L) of the gain medium are 1.518 and 11.5 mm, respectively. The index change results in a refraction of the input beam to a new tilt angle (α') of $\sim 0.54^\circ$. The beam waist size (w_c) at the center of the amplifier is 70 μm. The amplifier can be antireflection coated to prevent any unwanted reflections. The overall fiber-to-fiber distance of the system is ∼160 mm. In the simulation, seven angularly symmetrical cores are considered, as shown in Fig. 2(b). The independent beams from the seven-core fiber are spatially overlapped at the center

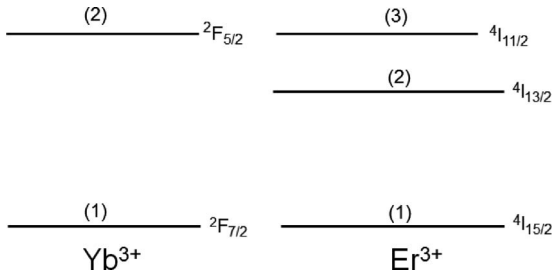

Fig. 3. Simplified energy level diagram of Yb–Er system.

of the gain medium in order to increase the overlap of the pump and signal. After amplification, the signal is spatially separated by using the second imaging system and coupled back to the output MCF. The amplifier can be side pumped or longitudinally pumped by using a single pump diode or an array of pump diodes. After amplification, the signal is spatially demultiplexed by using the second imaging system and coupled back to the output MCF.

3. Modeling of the Bulk Amplifier

Er^{3+} ions are used typically in fiber amplifiers due to the fact that their emission wavelength is located in the optical communication window. A typical EDF has a doping concentration around $20 \cdot 10^{24}$ Er^{+3} ions/m^3 [11], which can result in tens of decibels of gain over several meters. As the length of a bulk amplifier is much shorter (a few centimeters), much higher doping concentrations are needed in order to obtain high gain. However, cluster and ion pair phenomena limit the Er^{3+} doping concentration, which results in poor absorption of the pump light. To increase the pump absorption, Yb^{3+} ions are used with absorption cross section several times higher than Er^{3+} ions. Excited Yb^{3+} ions then transfer energy to the Er^{3+} ions. In our simulations, we chose Er–Yb ions in a phosphate glass host as its energy transfer efficiency is higher than that of other host materials [12].

The energy level diagram of an Er–Yb system is shown in Fig. 3.

A comprehensive explanation of the energy transfer process of the above system can be found in [12].

The population of the energy levels can be written as

$$N_{yb}^1 + N_{yb}^2 = N_{yb}^t \tag{1}$$

$$N_{er}^1 + N_{er}^2 + N_{er}^3 = N_{er}^t. \tag{2}$$

In the above equations, N_{yb}^1 and N_{yb}^2 are the Yb^{3+} ion populations at the lower and upper energy states; N_{er}^1, N_{er}^2, and N_{er}^3 are the Er^{3+} ion populations at the $^4I_{15/2}$, $^4I_{13/2}$, and $^4I_{11/2}$ energy levels; and finally, N_{er}^t and N_{yb}^t are the total doping concentrations of Er^{3+} and Yb^{3+} ions.

After applying the appropriate approximations about the energy level depletion and de-excitation rates that are listed in [13], the steady-state rate equations of the Er–Yb system can be simplified to

$$0 = \sigma_{yb} N_{yb}^t \Phi_p - k N_{yb}^2 \left(N_{er}^t - N_{er}^2\right) - \frac{N_{yb}^2}{\tau_{yb}} \tag{3}$$

$$0 = k N_{yb}^2 \left(N_{er}^t - N_{er}^2\right) - \sigma_{er}\left(2N_{er}^2 - N_{er}^t\right)\Phi_s - \frac{N_{er}^2}{\tau_{er}} \tag{4}$$

where, σ_{yb} is the ytterbium absorption cross section at the pump wavelength (σ_{yb} is $14.1 \cdot 10^{-21}$ cm^2 at 980 nm), and σ_{er} is the erbium emission cross section at the signal wavelength (σ_{er} is $8.0 \cdot 10^{-21}$ cm^2 at 1533 nm). Φ_p and Φ_s are the pump and signal photon fluxes, respectively. Note that the signal laser photon flux Φ_s is the total photon flux for all the seven signal beams. k is the energy transfer coefficient from $^2F_{5/2}$ to $^4I_{11/2}$, and τ_{yb} and τ_{er} are the lifetimes of the $^2F_{5/2}$ and

$^4I_{13/2}$ states of Yb^{3+} and Er^{3+} ions (τ_{yb} and τ_{er} are 2.125 and 7.5 ms, respectively, for the doping concentrations of Yb^{3+} and Er^{3+} used in this paper [14], [15]).

Similar to the way described in [16], [17], the above steady-state rate equations can be solved analytically to obtain the population inversion

$$\Delta N(x, y, z) = N_{er}^2(x, y, z) - N_{er}^1(x, y, z) \tag{5}$$

and the saturated gain coefficient is then

$$g(x, y, z) = \sigma_{er} \cdot \Delta N(x, y, z). \tag{6}$$

The saturated gain coefficient shown above can then be inserted into the following paraxial wave equation [16]:

$$2ik_0 n_0 \frac{\partial A(x, y, z)}{\partial z} = \frac{\partial^2 A(x, y, z)}{\partial x^2} + \frac{\partial^2 A(x, y, z)}{\partial y^2} + k_0^2 \left[i \frac{n_0}{k_0} g(x, y, z) + n^2(x, y, z) - n_0^2 \right] \cdot A(x, y, z). \tag{7}$$

In this equation, k_0 is the wavenumber in vacuum, n_0 is a reference refractive index, and n_0 was set to be the refractive index of the gain medium, which is 1.518; $n(x, y, z)$ was also assumed to be uniformly 1.518, which means that there is no thermal lensing or any other index perturbation in the gain medium. $A(x, y, z)$ is the slowly varying complex amplitude of the electric field for each of the seven continuous-wave (cw) signal laser beams.

The one-way propagation of each signal laser beam from each of the fiber cores through the bulk amplifier was calculated by numerically solving (7) [16]. The numerical one-way propagations of each of the seven beams need to be iterated with each other until the solution converges to the desired accuracy, in a way similar to that described in [16] and [17].

The numerical solution of the scalar paraxial wave equation shown in equation (7) was conducted in a way similar to that described in [16]. In the beam propagation method (BPM) calculation, the common finite-difference method was used for discretization in the transverse *xy* plane. The Crank–Nicholson scheme was used for discretization in the *z*-direction, which is the length of the gain medium. The saturated gain was accounted for by the same iterative method described in [16].

For the system considered in this paper, it is assumed that each core in the MCFs is a single-mode core. Therefore, ideally, the signal in each core of the MCF is an LP_{01} mode beam, which can be well approximated as a TEM_{00} Gaussian beam in free space after exiting the fiber.

In the simulation, the input signal beams at the input plane of the gain medium are all set to be TEM_{00} Gaussian beams, and all the outer input beams are shifted in different directions from the center of the input plane and are tilted so that all the signal beams overlap with each other at the center of the gain medium along the length, as can be seen in Fig. 2. In addition, the beam waists of all the signal beams used in the simulation including the central beam are at the center of the gain medium along the length, which is where all the signal beams overlap. All the signal beams are actually focused into the gain medium by the imaging system. In the simulation, the location of the beam waists and beam overlap at the center of the gain medium along the length are satisfied very well when there is neither gain nor absorption in the phosphate glass, and the beam waist radius is 70 μm for all the signal beams. The presence of gain in the phosphate glass changes the situation a little bit but not significantly.

The tilting of the outer input TEM_{00} Gaussian beams are realized by introducing a phase factor to each of the outer beams at the input plane of the phosphate glass gain medium, in a way similar to that described in [16] to account for curved laser cavity mirror.

So far, this imaging amplifier concept has only been investigated for cw signal lasers and cw pump. Short pulse amplification with high data rate systems needs more consideration, including the time-dependent gain dynamics, dispersion, and pulse broadening.

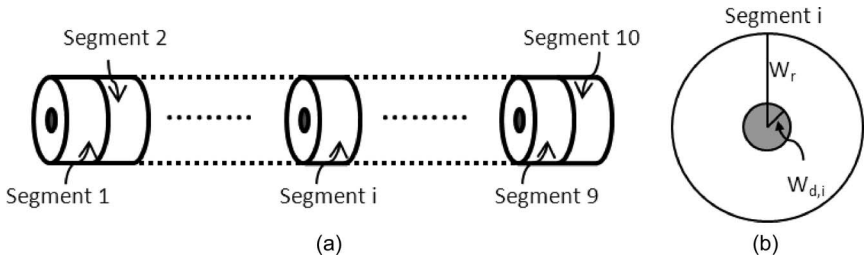

Fig. 4. Schematic of the gain medium design determined and used in the simulation. (a) View of the whole gain medium. (b) Cross-section view of the i_{th} piece (segment).

4. Gain Medium Design and Pumping Scheme

To be applied in the space-multiplexed optical transmission system, the optical power conversion efficiency (OPCE) for this imaging amplifier is an important factor. It is also very important that the signal after passing the bulk amplifier can be efficiently coupled back to the output MCF, which means that it is essential to maintain the intensity and phase profiles of the output signals as undistorted as possible, compared with the input signals.

Extensive simulation has been done to explore how to achieve these goals. It has been determined through simulation that absorbed pump distribution is important for improving the OPCE and reducing the distortion of the signal beams after passing through the bulk amplifier. The favorable absorbed pump distribution can be realized by properly designing the gain medium structure and side-pumping configuration.

Shown in Fig. 4 is a schematic of the gain medium design used in the simulation. The gain medium shown in Fig. 4 is essentially a composite laser rod, but it is different from the common composite laser rod. In Fig. 4(a) and (b), the shaded part (with radius of $w_{d,i}$ for the i_{th} piece) is phosphate glass doped with Er and Yb ions; the unshaded part (with outer radius of w_r) is undoped pure phosphate glass. From Fig. 4(a), it can be seen that the rod-shaped gain medium is composed of ten pieces (the number of pieces could be other than ten), with each piece having a structure shown in Fig. 4(b) (shown is the i_{th} piece). The outer radius w_r is the same for all the pieces, as shown in Fig. 4, but the radius of the doped region $(w_{d,1}, w_{d,2}, \ldots, w_{d,i}, \ldots)$ generally varies from piece to piece.

The side-pumping scheme is suitable for delivering the pump light from diode lasers into the gain medium, and diode lasers producing multiple spatial-mode output could be used as the pump source.

Using side pumping, it might be convenient to vary and adjust the pump power delivered to each piece (segment) of the gain medium, as sketched in Fig. 4. Therefore, the absorbed pump power can be conveniently controlled and adjusted as desired for each of the pieces of the gain medium.

One way to improve the pump absorption efficiency for side pumping is to use a side-pumping scheme similar to that described in [18]. Similar to the scheme shown in Fig. 4 in [18], if the cylindrical surface of the rod-shaped gain medium is highly reflective for pump light wavelength, except the entrance window for pump light, which is highly transmissive for pump light wavelength, it is possible for the pump light to bounce back and forth many times in the rod to increase the effective absorption length. Another way is to use oblique incidence for the pump along the gain medium. If we assume 60° oblique incidence for the pump, it is possible to reach 80% efficiency for double-pass pump absorption.

Simulation demonstrated that the performance of this amplifier could be optimized by properly adjusting different parameters for this amplifier system. These parameters include the thickness of each piece (segment), as shown in Fig. 4(a); the total length of the whole gain medium; the doping concentration; the radii of the regions doped with Er and Yb ions $(w_{d,1}, w_{d,2}, \ldots, w_{d,i}, \ldots)$ for different segments in the gain medium; the absorbed pump power in each piece of the gain medium; the transverse size of the signal beams; and the tilt angle for the outer signal beams.

As an approximation in the simulation presented here, it is assumed that the pump absorption efficiency is 100%, and the absorbed pump distribution is uniform in the doped region in the gain medium sketched in Fig. 4. Of course, in a practical amplifier system, the pump absorption efficiency will be less than 100%, and the absorbed pump distribution cannot be perfectly uniform.

In the simulated system, the OPCE can generally be improved if the gain medium closer to the output plane of the bulk amplifier is pumped harder than the gain medium closer to the input plane, with the total pump power fixed to a specific value. In addition, the transverse size of the gain region ($w_{d,1}, w_{d,2}, \ldots, w_{d,i}, \ldots$, the radii of the regions doped with Er and Yb ions) shall also be varied along the length of the gain medium, to better match the total intensity profile of all the signal beams. In addition, an unsymmetrical distribution of doped region radius $(w_{d,1}, w_{d,2}, \ldots, w_{d,i}, \ldots)$ along the length of the gain medium could also be helpful, and $w_{d,10}$ [for the last piece of the gain medium, segment 10 in Fig. 4(a)] is smaller than $w_{d,1}$ (for the first piece, segment 1 right beside the input plane). This nonuniform distribution of the transverse size of the gain region helps to further improve the OPCE and reduce the distortion of the signal beams after passing through the bulk amplifier.

Furthermore, increasing total pump power and total input power for all the signal beams (by increasing the input power for each signal beam or by increasing the number of cores and then number of signal beams, or both) is also a useful strategy to improve the optical power conversation efficiency, while maintaining the same amplification for each of the signal beams, e.g., 20 dB.

5. Simulation Results

We have simulated the amplification of a seven-core fiber for an input power of 6 mW from each individual core, which makes the total input power 42 mW. As an ideal case, which shall also be the upper limit for the practical case, it is assumed that the pump absorption efficiency is 100%, and the absorbed pump distribution is uniform in the doped region in the gain medium, as sketched in Fig. 4. By properly adjusting the different parameters for the considered amplifier system, the power conversion efficiency has been optimized greatly. In the simulated system, the gain medium closer to the output plane of the bulk amplifier is pumped harder than the gain medium closer to the input plane with the total pump power fixed to a specific value (15 W here). This nonuniform pump power distribution along the length of the gain medium can generally improve the power conversion efficiency. In addition, the transverse size of the gain region ($w_{d,1}, w_{d,2}, \ldots, w_{d,i}, \ldots$, the radii of the regions doped with Er and Yb ions) was varied along the length of the gain medium, and this resulted in better matching between the absorbed pump distribution and the total intensity profile of the seven signal beams. The concentration of erbium ions was determined to be 6.13×10^{26} ions/m^3 and that of the ytterbium ions was taken to be $1.5 \cdot 10^{27}$ ions/m^3. The length of the amplifier gain medium was determined to be 11.5 mm. This set of erbium and ytterbium doping concentrations is practical in this type of glass material [14], [15], and the pump absorption efficiency will be high in the practical amplifier system so long as proper side-pumping scheme and gain medium design are used to try to realize the absorbed pump distribution determined and used in the simulation.

The power evolution of the signal beams along the length of the amplifier gain medium given by the simulation is shown in Fig. 5 for a total pump power of 15 W. At the output of the bulk amplifier, the central beam is amplified to 742 mW, and the outer beams are amplified to 696 mW, which results in a $\sim$20.9-dB gain for the center core and a $\sim$20.6-dB gain for the outer cores. This corresponds to an overall OPCE of 32.5%. The signal from the center core experiences slightly higher gain than the other channels as the signal and pump overlap is maximum. The gain for the cores can be equalized by properly adjusting the parameters for this amplifier system, such as the absorbed pump distribution.

After amplification, the signals need to be coupled back to the individual cores by the second imaging system, *IS 2*. To do so, the amplified signal wavefront after amplification needs to be as undistorted as possible to reduce coupling loss. According to the simulation, the spatial phase degrades after the signal passes the gain medium. The spatial phase may also degrade due to any imperfections in a practical amplifier system. Shown in Fig. 6 is the difference between the phase of

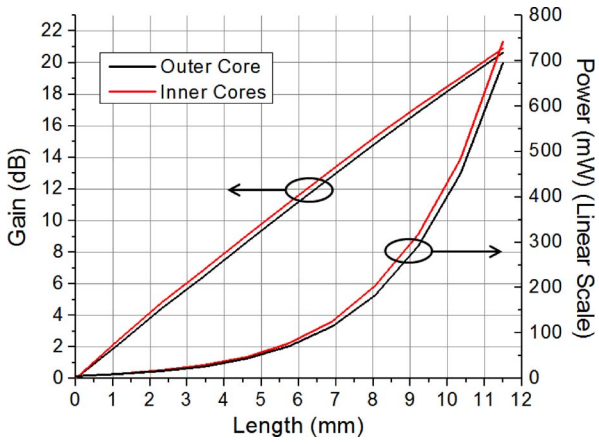

Fig. 5. Power evolution of the signals along the length.

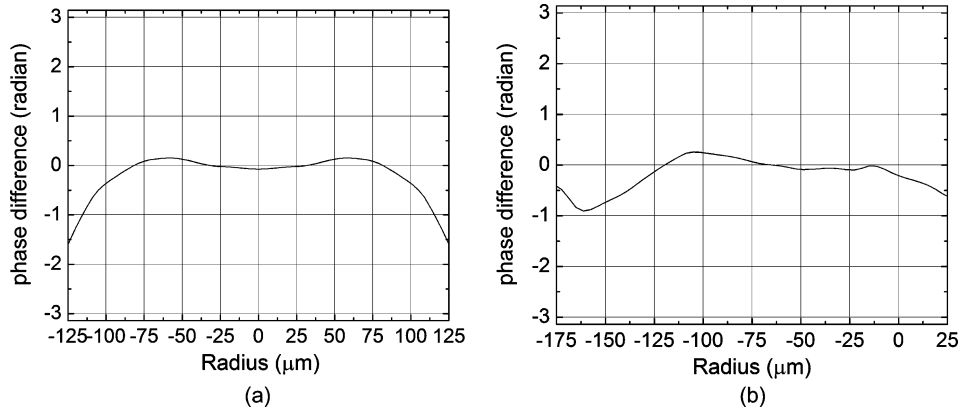

Fig. 6. Spatial phase difference of the center beam (a) and one of the outer beams (b). The phase difference here is the difference between the phase of the calculated output signal beam right after amplification and the phase of the same calculated output signal beam assuming that there is no doping in the phosphate glass medium (only pure phosphate glass), which means that there is neither gain nor absorption in the phosphate glass medium.

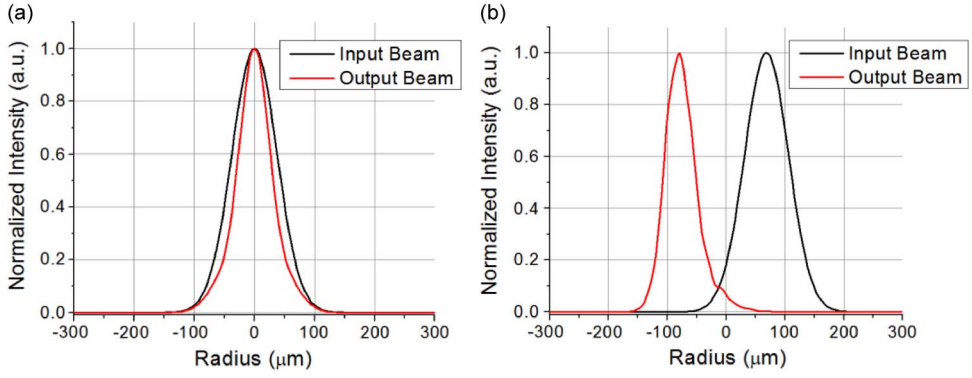

Fig. 7. Intensity profile of the center beam (a) and one of the outer beams (b) before and after the amplification.

the calculated output signal beam and the phase of the same calculated output signal beam but without gain or absorption in the medium (only pure phosphate glass assumed). Fig. 6(a) is the phase difference for the center beam, and Fig. 6(b) is the phase difference for one of the outer beams. In our system, the wavefront degradation might result from the narrow gain region and nonuniform gain saturation. The wavefront can be corrected easily by using a phase plate.

The intensity profiles of the center beam and one of the outer beams are also shown in Fig. 7(a) and (b). The intensity profile of the outer beam changes sides with respect to the center after passing the amplifier as expected. Both the outer and center beam intensity profiles also show some narrowing due to the gain dynamics of the bulk amplifier.

6. Discussions

The imaging amplifier method exploits the parallelism of bulk optics to provide the additional degrees of freedom necessary for the amplification of signals from multicore and multimode fibers. It is possible to build a multimode EDFA (simply by replacing the single-mode EDF with a multimode EDF) for optical transmission in MMF [19], [20]. Therefore, this method is more critically needed for optical transmission in systems employing MCF. The benefit of exploiting such parallelism is significant savings in component count in comparison with using dedicated EDFAs for each core [21]. With the added degrees of freedom, several potential disadvantages must be addressed. First is the noise figure of the imaging amplifier caused by the fact that the additional degrees of freedom in the bulk amplifier contain spontaneous emission. Fortunately, with the imaging system, only spontaneous emission contained in the signal modes will be coupled into the output fiber. Even if some spurious spontaneous emission not contained in the signal modes is coupled into the output fiber, it will not propagate in the output fiber. As a result, the fundamental noise figure of the imaging amplifier should still be 3 dB for each degree of freedom.

If there are more than seven cores in the MCF, for example, 19 cores or even more, and each core is a multimode one that can support several eigenmodes, the power conversion efficiency of this imaging amplifier could be even higher. Since increasing number of cores and number of eigenmodes supported by each core make it easy to further increase the total input power for all the signal beams, this is helpful to further increase the OPCE for this imaging amplifier as applied to space-multiplexed optical transmission system. According to our simulation, an OPCE as high as $\sim$50% might be achieved using this imaging amplifier, if there are 19 cores in the MCFs, with each core supporting several eigenmodes.

Another way to increase the total input power for all signal beams for this imaging amplifier is to add a preamplifier. If the power for each beam from each core of the MCF is 2 mW, which is typical for a large-channel-count WDM transmission system, it will not be difficult to amplify it to 16 mW using a preamplifier. The overall OPCE will be dominated by the power amplifier stage.

Compared with EDFAs, the potential benefits of this imaging amplifier concept are attractive. It is simple, since one imaging amplifier can be used to amplify signals from many cores, with each core supporting one or several spatial modes. If MCFs with more cores, and thus higher total input power, are used in space-multiplexed optical transmission, the OPCE can be increased further according to our simulation.

Furthermore, in the imaging amplifier, a rod-shaped gain medium can be used, and it can be side pumped using multiple spatial-mode diode lasers. Therefore, the pump power requirement for pumping the gain medium is easy to meet. The pump absorption efficiency will also be high in a practical imaging amplifier system.

The effects of heat deposition due to absorption of pump power are expected to be not significant. If necessary, conductive cooling using a copper heat sink might be a good way to remove the deposited heat in the gain medium [22].

As for amplified spontaneous emission, since there is no waveguide in the imaging amplifier, as is the case for EDFAs, it needs more investigation to see if there are any advantages using this imaging amplifier scheme.

Finally, there might be more room for further improvement of the performance of this imaging amplifier concept, and more advanced designs still need to be pursued.

7. Conclusion

In this paper, we propose a novel amplification method for spatially multiplexed fibers. The proposed method was simulated for a seven-core fiber using an Er–Yb phosphate glass as the amplifying region. A ~20-dB gain of the input signal and 32.5% OPCE for a seven-core MCF were obtained in the simulation with 15-W pump power. We believe the proposed imaging amplifier technique has the potential to increase the signal reach in a practical manner for the long-haul optical transmission systems.

References

[1] S. Kawanishi, H. Takara, K. Uchiyama, I. Shake, and K. Mori, "3 Tbit/s (160 Gbit/s × 19 channel) optical TDM and WDM transmission experiment," *Electron. Lett.*, vol. 35, no. 10, pp. 826–827, May 1999.

[2] W. Shieh, H. Bao, and Y. Tang, "Coherent optical OFDM: Theory and design," *Opt. Exp.*, vol. 16, no. 2, pp. 841–859, Jan. 2008.

[3] K. Roberts, M. O'Sullivan, K.-T. Wu, H. Sun, A. Awadalla, D. J. Krause, and C. Laperle, "Performance of dual-polarization QPSK for optical transport systems," *J. Lightw. Technol.*, vol. 27, no. 16, pp. 3546–3559, Aug. 2009.

[4] E. Ip, A. P. T. Lau, D. J. F. Barros, and J. M. Kahn, "Coherent detection in optical fiber systems," *Opt. Exp.*, vol. 16, no. 2, pp. 753–791, Jan. 2008.

[5] G. Li, "Recent advances in coherent optical communication," *Adv. Opt. Photon.*, vol. 1, no. 2, pp. 279–307, Apr. 2009.

[6] T. S. S. Inao, S. Sentsui, T. Kuroha, and Y. Nishimura, "Multicore optical fiber," presented at the Optical Fiber Commun. OSA Techn. Dig. Ser., Washington, DC, 1979, Paper WB1.

[7] R. Ryf, S. Randel, A. H. Gnauck, C. Bolle, R. Essiambre, P. J. Winzer, D. W. Peckham, A. McCurdy, and R. Lingle, "Space-division multiplexing over 10 km of three-mode fiber using coherent 6 × 6 MIMO processing," presented at the Optical Fiber Commun. Conf. Exp./Nat. Fiber Optic Engineers Conf., Los Angeles, CA, 2011, Paper PDPB10.

[8] F. Yaman, N. Bai, B. Zhu, T. Wang, and G. Li, "Long distance transmission in few-mode fibers," *Opt. Exp.*, vol. 18, no. 12, pp. 13 250–13 257, Jun. 2010.

[9] B. Zhu, T. Taunay, M. Fishteyn, X. Liu, S. Chandrasekhar, M. Yan, J. Fini, E. Monberg, F. Dimarcello, K. S. Abedin, P. W. Wisk, D. W. Peckham, and P. Dziedzic, "Space-, wavelength-, polarization-division multiplexed transmission of 56-Tb/s over a 76.8-km seven-core fiber," in *Optical Fiber Communication Conf. Exposition (OFC/NFOEC)/Nat. Fiber Optic Engineers Conf.*, Los Angeles, CA, 2011, Paper PDPB7.

[10] S. Jun, A. Yoshinari, W. Naoya, K. Atsushi, K. Tetsuya, H. Tetsuya, T. Toshiki, K. Tetsuya, and W. Masayuki, "109-Tb/s (7 × 97 × 172-Gb/s SDM/WDM/PDM) QPSK transmission through 16.8-km homogeneous multi-core fiber," presented at the Optical Fiber Commun. Conf. Exp./Nat. Fiber Optic Engineers Conf., Los Angeles, CA, 2011, Paper PDPB6.

[11] P. Myslinski, C. Szubert, A. J. Bruce, D. J. DiGiovanni, and B. Palsdottir, "Performance of high-concentration erbium-doped fiber amplifiers," *IEEE Photon. Technol. Lett.*, vol. 11, no. 8, pp. 973–975, Aug. 1999.

[12] S. Taccheo, P. Laporta, S. Longhi, O. Svelto, and C. Svelto, "Diode-pumped bulk erbium–ytterbium lasers," *Appl. Phys. B, Lasers Opt.*, vol. 63, no. 5, pp. 425–436, Nov. 1996.

[13] E. Tanguy, C. Larat, and J. P. Pocholle, "Modelling of the erbium–ytterbium laser," *Opt. Commun.*, vol. 153, no. 1–3, pp. 172–183, Jul. 1998.

[14] R. Wu, J. D. Myers, M. J. Myers, and C. Rapp, "Fluorescence lifetime and 980 nm pump energy transfer dynamics in erbium and ytterbium co-doped phosphate laser glasses," in *Proc. SPIE*, 2003, vol. 4968, pp. 11–17.

[15] *Technical Document*, Kigre, Inc., Hilton Head, SC, 1990.

[16] H. Shu and M. Bass, "Three-dimensional computer model for simulating realistic solid-state lasers," *Appl. Opt.*, vol. 46, no. 23, pp. 5687–5697, Aug. 2007.

[17] H. Shu, Y. Chen, M. Bass, J. F. Monjardin, and J. Deile, "Numerical modeling of alkali vapor lasers," *Opt. Exp.*, vol. 19, no. 21, pp. 19 875–19 885, Oct. 2011.

[18] W. Hageman, Y. Chen, X. Wang, L. Gao, G. U. Kim, M. Richardson, and M. Bass, "Scalable side-pumped, gain-guided index-antiguided fiber laser," *J. Opt. Soc. Amer. B*, vol. 27, no. 12, pp. 2451–2459, Dec. 2010.

[19] N. Bai, E. Ip, T. Wang, and G. Li, "Multimode fiber amplifier with tunable modal gain using a reconfigurable multimode pump," *Opt. Exp.*, vol. 19, no. 17, pp. 16 601–16 611, Aug. 2011.

[20] P. M. Krummrich, "Optical amplification and optical filter based signal processing for cost and energy efficient spatial multiplexing," *Opt. Exp.*, vol. 19, no. 17, pp. 16 636–16 652, Aug. 2011.

[21] K. S. Abedin, T. F. Taunay, M. Fishteyn, M. F. Yan, B. Zhu, J. M. Fini, E. M. Monberg, F. V. Dimarcello, and P. W. Wisk, "Amplification and noise properties of an erbium-doped multicore fiber amplifier," *Opt. Exp.*, vol. 19, no. 17, pp. 16 715–16 721, Aug. 2011.

[22] W. Koechner, *Solid-State Laser Engineering*. New York: Springer-Verlag, 1999.